Review

Check for updates

doi.org/10.1002/tcr.202400016 tcr.wiley-vch.de

THE CHEMICAL RECORD

An Emerging Trend in the Synthesis of Iron Titanate Photocatalyst Toward Water Splitting

Moses D. Ashie, [a] Dhananjay Kumar, [b] and Bishnu Prasad Bastakoti*[a]

Abstract: Hydrogen gas is a prominent focus in pursuing renewable and clean alternative energy sources. The quest for maximizing hydrogen production yield involves the exploration of an ideal photocatalyst and the development of a simple, cost-effective technique for its generation. Iron titanate has garnered attention in this context due to its photocatalytic properties, affordability, and non-toxic nature. Over the years, different synthesis routes, different morphologies, and some modifications of iron titanate have been carried out to improve its photocatalytic performance by enhancing light absorption in the visible region, boosting charge carrier transfer, and decreasing recombination of electrons and holes. The use of iron titanate photocatalyst for hydrogen evolution reaction has seen an upward trend in recent times, and based on available findings, more can be done to improve the performance. This review paper provides a comprehensive overview of the fundamental principles of photocatalysis for hydrogen generation, encompassing the synthesis, morphology, and application of iron titanate-based photocatalysts. The discussion delves into the limitations of current methodologies and present and future perspectives for advancing iron titanate photocatalysts. By addressing these limitations and contemplating future directions, the aim is to enhance the properties of materials fabricated for photocatalytic water splitting.

Keywords: Iron titanate, Photocatalyst, Water splitting, Renewable energy, Hydrogen production

1. Introduction

Urbanization and rapid industrialization are giving rise to high demand for energy. Currently, most of the energy used is from fossil fuels and other natural sources which are not renewable.

[a] M. D. Ashie, Dr. B. P. Bastakoti

Department of Chemistry, North Carolina Agricultural and Technical State University, 1601 E. Market St, Greensboro, NC-27411, USA

E-mail: bpbastakoti@ncat.edu

[b] Dr. D. Kumar

Department of Mechanical Engineering, North Carolina Agricultural and Technical State University, 1601 E. Market St, Greensboro, NC-27411, USA

© 2024 The Authors. The Chemical Record published by The Chemical Society of Japan and Wiley-VCH GmbH. This is an open access article under the terms of the Creative Commons Attribution License, which permits use, distribution and reproduction in any medium, provided the original work is properly cited.

Increasing demand for crude oil, which is non-renewable, has prompted the need for recent advances in the search for renewable energy. [1] Many efforts have been made to generate fuel from more renewable energy sources such as wind, sun, bioenergy, and geothermal energy. Hydrogen gas generation has been one of the target areas for renewable and environmentally safe energy². Hydrogen production is carried out through processes such as (a) photocatalytic water splitting, (b) electrolysis of water, (c) thermochemical water splitting, and (d) photo-biological hydrogen production. [3] Hydrogen production from sunlight and water using solar photocatalytic water is considered a favorable solution to a more sustainable energy. [4]

Exploiting hydrogen gas as an energy source has advantages such as release of only water as a by-product, and has the highest energy density by weight as compared to other fuels. [5] Hydrogen gas has demonstrated a high energy capacity of 143 MJ/kg as compared to fossil fuel in the range of 44 to 55 MJ/kg and lithium-ion battery of 0.46 to 0.72 MJ/kg. [6]

Energy density, [7] which explains the amount of energy that has been stored in a material or a system per unit volume, aids in comparison of efficiency of those materials. Figure 1 shows the energy densities of some hydrocarbons and hydrogen gas. Calorific value, usually expressed in joules per kilogram, which is a measure of the energy contained in a fuel shows that hydrogen gas has high energy density. [8] The calorific value is determined by measuring the heat produced when a specified quantity of the fuel is combusted. Typical batteries utilize about 0.24 kWh to 0.87 kWh of electricity per mile. [9] This

was confirmed by the comparison of hydrogen and lithium made into a battery; reporting greater energy density of hydrogen batteries of about 40 kWh/kg, $^{[10]}$ higher than the lithium-ion battery energy density of about 0.25 kWh/kg and fuel oil of about 12 kWh/kg. 1 kg of a lithium battery can store only 0.15–0.25 kWh of electricity, while one kg - of hydrogen contains 39.6 kWh. $^{[9]}$



Mr. Moses Ashie is a PhD student in the Department Chemistry at North Carolina A&T State University. He gained his BSc in Chemistry from Kwame Nkrumah University of Science and Technology, Ghana. He is investigating the fabrication of inorganic materials with the aim of fabricating ideal photocatalysts, and exploring innovative techniques and instrumentation for effective hydrogen evolution. He is aiming to gain adequate knowledge in semiconductor nanomaterial synthesis with enhanced photocatalytic properties, characterization, and high yield application in photocatalytic hydrogen evolution through water splitting.



Dr. Dhananjay Kumar is an Oak Ridge National Laboratory (ORNL) Professor in the Department of Mechanical Engineering at North Carolina Agricultural and Technical State University (NCAT). Dr. Kumar obtained his Ph.D. degree in Chemistry from the Indian Institute of Technology, Bombay, in 1994. His research interests include innovative synthesis, electronic materials, magnetoresistance, superconductivity, fundamentals of thin film growth, and advanced materials processing. Recently, Dr. Kumar's group at NCAT has championed a new concept of bandgap engineering of transition metal oxides in low-dimensional geometries for water-splitting. Dr. Kumar is currently heading two centers at NCAT: Center for Electrochemical Dynamic and Reactions on Surfaces (funded by US DOE, #DE-SC0023415) and Collaborative Research and Education in Energy Materials (funded by US NSF, #2122067).



Dr. Bishnu Bastakoti pursued a PhD at Saga University, Japan as a Monbukagakusho scholar. Following this, he joined the National Institute for Materials Science as a JSPS Fellow. He previously worked at the University of Sydney and Harvard University before starting his independent career at North Carolina A&T State University. He is exploring a broad design challenge to control multiple structural properties such as porosity, crystallinity, and the dimension of porous inorganic nanomaterials. He is particularly interested in using highly porous nanostructured materials in catalysis and energy conversion.

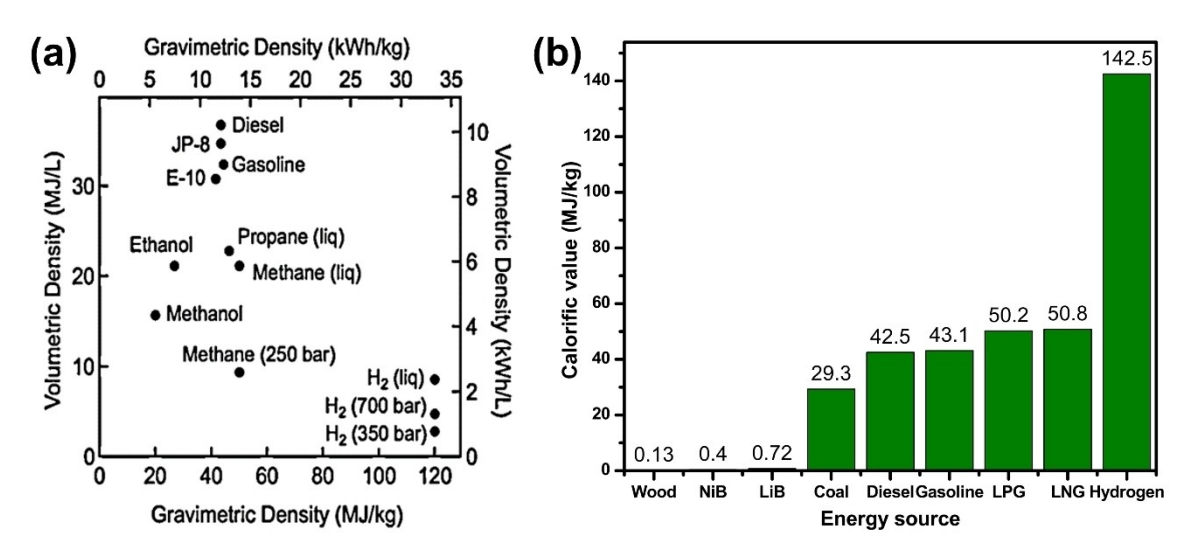


Figure 1. (a) Specific energy comparison of hydrogen gas (energy per mass) and energy density (energy per volume) for some fuel materials. Reprinted with permission from ref [7]. (b) Calorific values of some energy sources (NiB - Nickel metal hydride battery, LiB – lithium-ion battery). Reprinted with permission from ref [10].

1.1. The Need for Photocatalysts for H₂ Generation

Catalysts over the years have played a vital role in finding solutions to most environmental challenges. Various applications include but not limited to H₂ gas evolution, ^[2] CO₂ reduction, ^[11] dye degradations, ^[12] and water treatment ^[13] have been successful though continuous advancements are being made. Most of the materials used over the years have demonstrated the ability to function as catalysts though some of them have limitations. Limitations such as low yield, high-cost catalyst such as platinum, use of ultraviolet radiation, high operational energies, and less abundance. A major disadvantage for most catalysts intended for use in hydrogen production is due to the location of the conduction band (CB) which must be located at more negative potentials compared to the redox potential of H₂O reduction. ^[14] Other catalysts have fast electron-hole recombination and low electron densities.

Advantages in recent use of iron and titanium containing catalyst in photocatalysis is due to its relative abundance, low-cost and non-toxicity and suitable band gap to absorb the light. The relative abundance of iron and titanium in earth's crust are 56000 mg/L and about 5500 mg/L respectively. [15] Ilmenite (FeTiO₃) which serves as ore for TiO₂, is the starting material for about 93% of the global titanium demand. [16,17] TiO₂ has been frequently used as a photocatalyst but has a high band gap of about 3.0 eV (rutile) or 3.23 eV (anatase) which limits its application in solar light as explained by Fujishima and Honda. [18,19] This has given rise to the modification and synthesis of varieties of TiO₂ based catalyst. [20,21] Some of these modifications include the synthesis of ternary, quaternary, composite, and heterogeneous photo-

catalysts. Doping, and tuning shape, size, and porosity have also been an area of concern. Some photocatalysts developed in recent years include hematite (Fe₂O₃) which can absorb in the visible-light region and prevent electron-hole recombination and has been recently used in photocatalysis. Having a band gap of 2.1–2.2 eV, Fe₂O₃ has also been a promising catalyst for photocatalysis due to its ability to absorb light up to 600 nm. ^[22] Iron has gained attention recently due to better stability in an oxidative environment, abundance, and low cost in fabrication. The introduction of iron into TiO₂ for example reduces its bandgap from 3.2 eV to a bandgap to \approx 2.1 eV. ^[23]

In recent times, Centurion et al. [24] and Imrich et al. [25] reviewed the potential of pseudobrookite Fe₂TiO₅ for solar water splitting systems. The reviews by Rafique et al., [26] Amika et al., [27] Do et al. [28] and Aljar et al. [29] focused on TiO₂-based photocatalysts; less emphasis was made concerning iron titanate for photocatalytic activities. Thus, the present review article on the synthesis and photocatalytic properties of iron titanate is expected to be useful for the researchers in the field.

This review seeks to investigate the advances made in the use of iron titanate as a photocatalyst and future improvements that can be made to increase yield in its application. Lots of research has been conducted in the use of iron titanate nanoparticles in hydrogen production over the years. This review will first outline the basic principles of photocatalysis. Secondly, various synthesis techniques for iron titanate will be summarized. Thirdly, various experimental yields in the application of the catalyst will be explored in previous articles. Finally, outcomes of previous works will be discussed and summarized based on which future perspectives or future research areas will be identified. The voluminous articles from

15280691, 2024, 5, Downloaded from https://onlinelibrary.wiley.com/doi/10.1002/tcr.202400016 by Bishnu Bastakoti - North Carofina A&T State University , Wiley Online Library on [05/08/2025]. See the Terms and Conditions (https://onlinelibrary.wiley.

of use; OA articles are governed by the applicable Creative Commons I

the search results were narrowed through the use of "Iron titanate nanoparticles for hydrogen production through water splitting in the presence of light" as key terms in the search (Figure 2).^[30]

1.2. Properties of Iron Titanate

Though TiO₂ is an n-type semiconductor,^[31] Nowotny et al. has confirmed that FeTiO₃ shows a p-type conductivity behavior due to the contribution of Fe in the lattice structure.^[32–35] They also investigated the possible control of the properties of TiO₂ to form either p-type or n-type semiconductor material depending on the dopant/impurity concentration and controlled oxygen activity. Varying oxygen

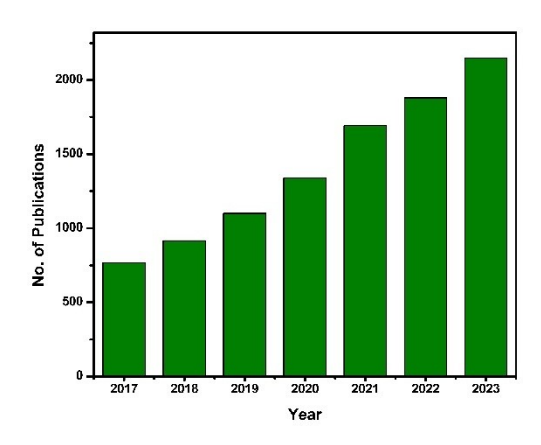


Figure 2. A number of publications on iron titanate in water-splitting applications. [27]

activity, concentration of aliovalent ions such as Fe with oxidation states of Fe2+ ions and Fe3+ ions, can cause the properties to change between n-type quasi-metallic conductors and p-type semiconductors. [36] With oxygen having an O²⁻ charge, FeTiO₃ is a stable compound with Fe²⁺ ions and Ti⁴⁺ ions oxidation states. FeTiO₃ is an oxide of iron and titanium and the most abundant crystal structure (Figure 3). Based on synthesis conditions and methods, different crystal lattices and molecular formulas may be formed with Fe_xTi_yO_z general formular. Fe₂TiO₅, Fe₂TiO₇, Fe₂Ti₃O₉, Fe₉TiO₁₅ and FeTiO₄ are some other possible molecular formulas with different crystal structure. [8,37-41] These titanates have been experimentally identified to have many applications; among them, photocatalytic activity FeTiO3 can reduce CO2 reduction to CH₃OH and other products, [42] and decomposition and degradation reactions.[43]

2. Principles of Photocatalysis Water Splitting for H₂ Generation

The fundamental principles governing the generation of hydrogen gas from water using semiconductors in light relate to the splitting of water molecules by a selective catalyst capable of exciting electrons in the presence of light of particular wavelength. When the light of sufficient energy equivalent to or greater than the band gap of semiconductor photocatalysts strikes the surface of the semiconductor, there will be excitation of electrons from the VB to the CB creating a hole in the VB. A potential difference is created between them resulting in reduction and oxidation reactions occurring

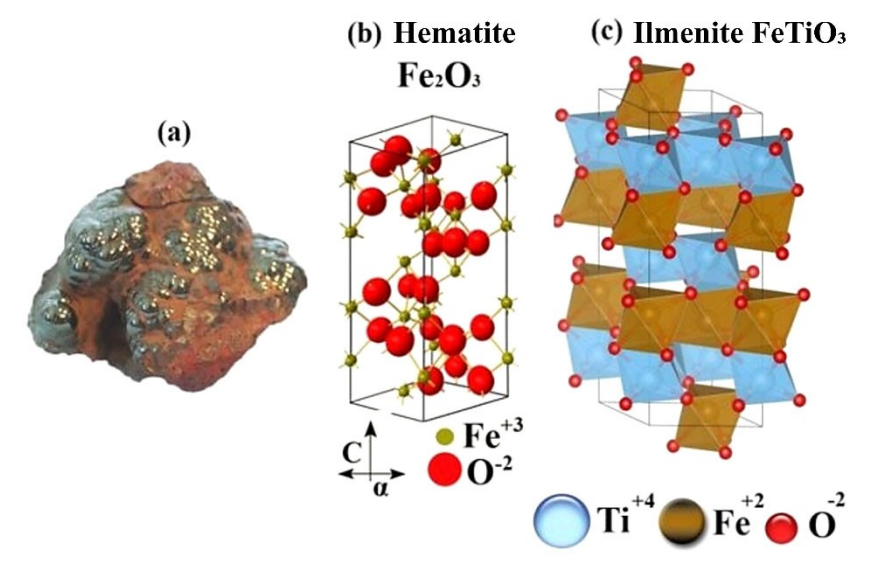


Figure 3. (a) Hematite ore (b), arrangement of ions of the rhombohedral hematite crystal with a corundum structure, (c) hexagonal arrangement of the metal cations in ilmenite. [35]

15280691, 2024, 5, Downloaded from https://onlinelibrary.wiley.com/doi/10.1002/trc.202400016 by Bishnu Bastakoti - North Carolina A&T State University, Wiley Online Library on [0508/2025]. See the Terms and Conditional Con

of use; OA articles are governed by the applicable Creative Commons I

at CB and VB respectively. Holes in the valence band will oxidize the water molecules to form oxygen while electrons will reduce the H⁺ ions to produce hydrogen in the CB. As shown in Figure 4, absorption of photons with energies exceeding the semiconductor band gap leads to the generation of electron (e—) and hole (h+) pairs in the semiconductor particles. There is charge separation followed by migration of photogenerated charge carriers in the semiconductor particles then finally the surface chemical reactions (oxidation and reduction) between these carriers with water molecules. Electrons and holes may also recombine with each other without participating in any chemical reactions. For effective photocatalyst, the energetic position of the bottom of the conduction band must be more negative than the reduction potential of water to produce H₂. [44]

2.1. Photocatalytic Water Splitting

Photocatalytic water splitting involves use of photocatalyst placed in a liquid medium and the use of chemical energy obtained from light to split water according to the reaction below. Tahir et al. described the water splitting is an endothermic process with Gibbs free energy change of about 237 kJ/mol.^[45]

$$H_2 O \to H_2 + \frac{1}{2}O_2; \ \Delta G = 237 \ kJ \ / \ mol$$
 (1)

The light must be of sufficient energy equal to or greater than the band gap of photocatalysts and this light is converted to chemical energy when it strikes the surface of semiconductor to initiate the generation of electron hole pairs for water splitting reaction. ^[46]

2.2. Photoelectrochemical Water Splitting

Photoelectrochemical (PEC) water splitting involves the use of light-responsive photocatalytic semiconductors as photocathodes, photoanodes, or both to generate charge carriers for photocatalytic activity. In comparison, PEC systems are more cost-effective than electrocatalytic (EC) systems which are complex with high-energy barriers, large overpotentials, and high electricity consumption. PEC process occurs without external bias when nanocatalysts with the right band gap are used. Zhang et al. constructed a photoelectrode- photovoltaic tandem device having two light absorbers to experiment the photocatalytic activity of synthesized materials. [47] Observation made by Ros et al. shows that holes are driven to photoelectrode's surface for oxygen evolution at the photoanode, and electrons are collected after closing the circuit for proton reduction to yield H₂ gas. [48] Zhang et al. investigated the effect of compositional ratio of metal oxides on photoelectrochemical process the interfacial layer between TiO2 and Fe2O3 helps to reduce the resistance between the heterogeneous interfaces. [49] In summary, three main processes of photoelectrochemical water splitting reaction as shown schematically in Figure 5 involve:

- (i) Photons from light cause photoexcitation of electrons after absorption of light by the semiconductor leading to the generation of electrons and holes,
- (ii) Separation of photogenerated electrons and holes (charge carriers), and their effective migration towards the surface of the semiconductor photocatalyst,

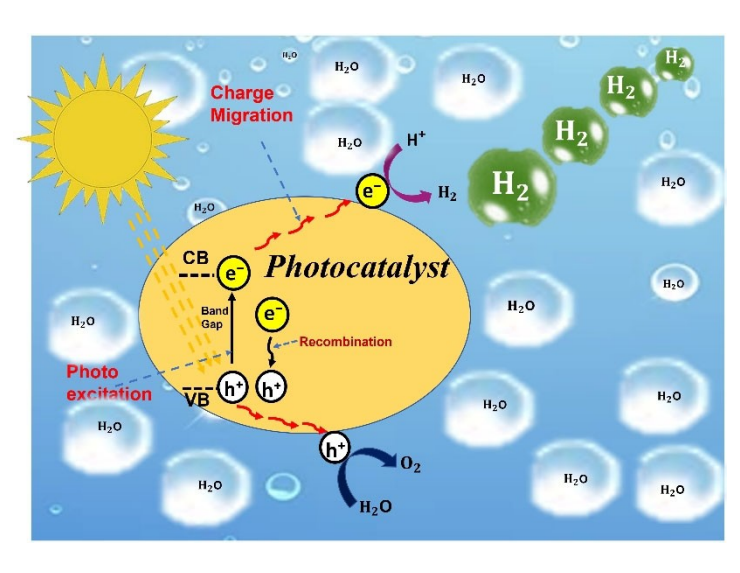


Figure 4. Mechanism of photocatalysis of water.

15280691, 2024, 5, Downloaded from https://onlinelibrary.wiley.com/doi/10.1002/tcr.202400016 by Bishnu Bastakoti - North Carolina A&T State University, Wiley Online Library on [0508/2025]. See the Terms and Conditions

of use; OA articles are governed by the applicable Creative Commons I

Figure 5. Photoelectrochemical generation of hydrogen gas.

(iii) The trapping of electrons and holes by the reaction sites for water oxidation and water reduction reaction as shown in equations.

$$2H_2 O \rightarrow 4H^+ + O_2 + 4e^- Oxidation (Anode)$$
 (2)

$$4H^+ + 4e^- \rightarrow 2H_2$$
 Reduction (Cathode) (3)

Electrons and holes which recombine in the bulk of photocatalyst semiconductor or on its surface releases the energy into the system in the form of heat or photons while electrons and holes that effectively migrate without recombination undergoes reduction and oxidation of the reactants in contact with the photocatalyst semiconductor.^[50]

3. Synthesis of Iron Titanate-Based Nanoparticles

Recent synthesis procedures employ both bottom-up and topdown approaches. [51,52] Synthesis of FeTiO₃ nanoparticles (NPs) employs bottom-up approach usually in the presence of surfactants to achieve segregated materials with high surface area and sometimes porous. [53-55] Most literature reviewed in this study used a bottom-up approach to fabricate NPs from their molecular or ionic precursors to the formation of crystals. The surfactants assist in controlling morphology and generating pores. [56] Diana et al. used top-down approach to synthesize FeTiO3 NPs by milling the ilmenite concentrate and photocatalytic activity was enhanced by modification with Mg and MgO^[2]. Electromagnetic and dry magnetic separation was used to obtain pure grains which were milled together with the composite precursor, Mg or MgO. Each method employs reaction conditions such as temperature, pH and calcination temperatures that must be monitored to achieve desired morphology. Most iron titanate NPs have been synthesized through methods such as sol-gel, self-assembly, hydrothermal/solvothermal and other simple techniques which have been highlighted in the subsections below.

3.1. Sol-gel Method

Yilmaz et al. reported that nanomaterial synthesis using sol-gel method yields more stable particle surfaces and high surface area with improved chemical and physical properties. [57] Sol-gel technique also referred to as chemical solution deposition is a wet chemical process employing hydrolysis and polycondensation steps in the synthesis process (Figure 6). Gelation, aging, drying, densification, and finally crystallization process follows in sequence. As illustrated in Figure 6A, the layered FeTiO₃ (L-FTO) used as anode material for quasi-solid-state sodium ion capacitor was formed by solvothermal route and the sodium ions conducting gel polymer membrane synthesized by sol-gel method. Liu et al. used a polyvinylidenediflouride-cohexafluoropropylene (VDF-HFP) as copolymer in the membrane synthesis, which were dissolved to form a sol, gelatinized, dried and the resulting solid membrane immersed in a sodium-containing organic electrolyte for sodium infusion. [58] This synthesis process resulted in an effective fabrication of sodium ion capacitor. Sol-gel technique is a process where the precursor is hydrolyzed in the acidic or basic mediums followed by polycondensation of the hydrolyzed products as the two major steps. The technique forms solid nanoparticles

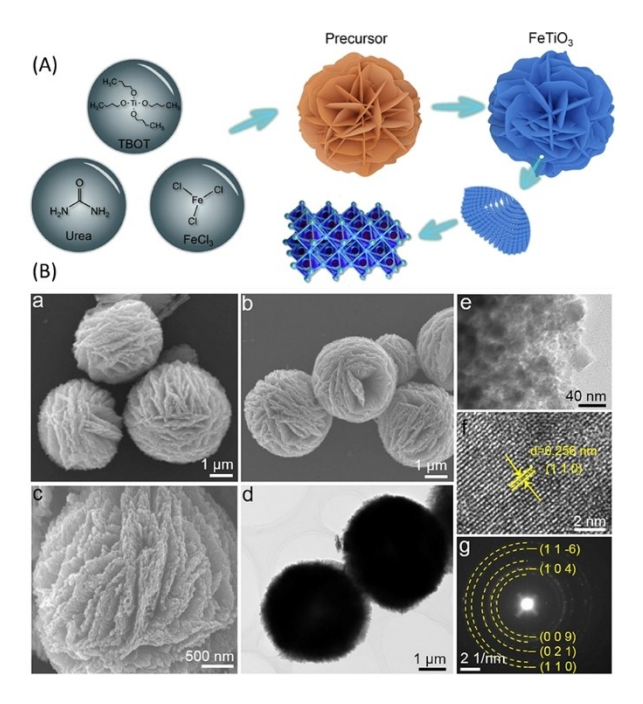


Figure 6. (a) Synthesis and (b) Morphology of multi-layered $FeTiO_3$ nanostructures. [58]

15280951, 2024, 5, Dowloaded from https://olinietbrary.wiely.com/doi/10.002/tr.202400016 Bishnu Bastaktai-North Carolina A&T State University, Wiley Online Library of [05/08/2025]. See the Terms and Conditions (https://olinietibrary.viely.com/terms-and-conditions) on Wiley Online Library for rules of use; OA archies are governed by the applicable Creative Commons L

which are dispersed in the liquid (sol), agglomerates and forms a continuous three-dimensional (3D) network resulting in the formation of a gel. Morphology and properties of nanoparticles are effectively improved when synthesis conditions such as pH, temperature and agitation are well controlled. The sol-gel selfassembly method was used to synthesize Fe₂TiO₅ nanoparticles which were loaded on a fluorine-doped tin oxide substrate containing a GaO₃ underlayer. Fe₂TiO₅ was successfully synthesized using self-assembly of opal templates made up of polystyrene (PS) spheres of 250 nm diameter which exhibited high charge mobility and enhanced visible light absorption properties. [59] Sol-gel method successfully used in the synthesis of a-Fe₂O₃/Fe₂TiO₅/Co-Pi, [60] Fe₂TiO₅/FeOOH, [59] TiO₂/ Fe_2TiO_5/Fe_2O_{3} , [49] Fe_2TiO_5/TiO_2 [38] composites, Fe_2TiO_2 , [61] Si/Fe-TiO₂, [62] Co-doped Fe₂TiO₅. [63] These compositions showed an improved photoelectrochemical and optical properties as compared to their pristine samples. This method serves as an easy-to-control morphology and particle sizes through adjustment of synthesis procedures. It is easy to incorporate dopants and engineering of composite materials on a nanoscale. However, synthesis duration and monitoring can sometimes be longer compared to other synthesis methods. It is sometimes difficult to find suitable solvents and adjust the reaction conditions.

3.2. Hydrothermal/Solvothermal Method

The hydrothermal synthesis yields excellent crystals through chemical reactions in a sealed vessel which is heated under temperatures above ambient temperature and pressure (Figure 7). Hydrothermal method has been reported to be suitable in controlling the nucleation and growth of nanoparticles through the use of suitable surfactants, ligands and control of pH of the reaction medium.^[64] Though in situ monitoring of reaction progress is difficult, hydrothermal technique has been reported to achieve in good dispersibility of particles in

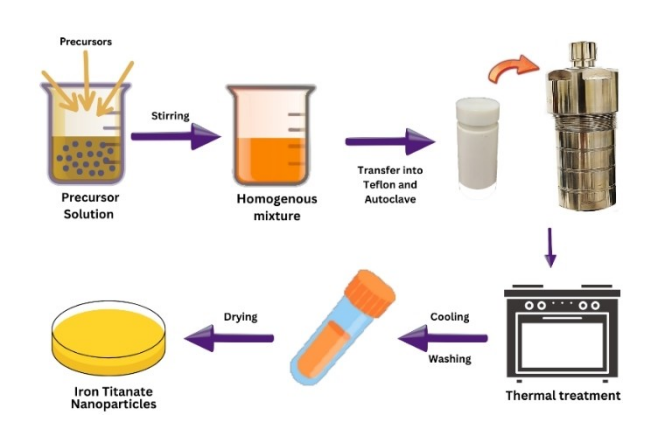


Figure 7. Schematic representation of hydrothermal /solvothermal technique.

solvents.. [65] Bassi et al. synthesized Fe₂TiO₅ using solvothermal method on FTO substrates and doped with SnO_x via surface treatment using 20 mM SnCl₄·5H₂O solution to form thin films, exhibiting good catalytic properties comparable to hematite for photoelectrochemical cell applications. [66] Co/Fe-Ti₂O₇ nanotubes were synthesized by hydrothermal method. and Fe and Co doped using simple ion exchange technique. The addition of iron and cobalt into the titanate lattices substantially enhanced photocatalytic performance due to reduced band gap and improved light absorption properties. [19] The hydrothermal method resulted in the formation of TiO₂ nanowires which have high surface area. [14] The TiO2 nanowires served as a primary framework in loading Co, Fe and layered double hydroxide using Co(NO₃)₂.6H₂O and Fe-(NO₃)₃.9H₂O precursors by simple ultrasonication and stirring. The hydrothermal and solvothermal method aided in the synthesis of different iron titanate compositions including, 2D graphene-assisted low-cost metal (Ag, Cu, Fe, or Ni)-doped TiO₂ nanowire (GP/M/TNW) architectures, [67] BiVO₄/ Fe-Ag/TiO₂, [70] Fe₂TiO₅-TiO₂, [71] Fe-Ni/TiO₂. [72] The making of composites resulted in the various morphologies having enhanced optical and electronic properties required for photocatalytic hydrogen generation activities. This synthesis technique provides good control over the size, shape, and porosity of the materials, and synthesis conditions such as temperature and pressure can easily be controlled. However, this technique can result in poor solution homogeneity affecting reproducibility and crystal growth monitoring and can be expensive in terms of instrumentation and energy requirement.

3.3. Electrospinning Method

The electrospinning involves an electrohydrodynamic method where a droplet of liquid is electrified to generate a jet. The technique is generally known to yield fibrous nanoparticles. Stretching and elongation steps follow to generate nanofibers. Carbon nanofibers (CNFs) decorated with heterojunction of FeTiO₃/TiO₂ nanoparticles were synthesized using electrospinning method. [73] Sharma et al. reported the electrospinning synthesis technique as a voltage-driven process which uses an electro-hydrodynamic method requiring the application of a high voltage to a polymer solution. The process is followed by the electrification of the liquid droplets to generate a jet. Finally, the jet is elongated and stretched to form fibers. [74] The magnetron-sputtering technique was successfully used to synthesize indium-tin-oxide/titanate (ITO/Fe₂TiO₅)^[75] and Ag/TiO₂/Fe₂TiO₅ composite synthesized using electrospinning technique, [37] all showing improved photocatalytic activity as compared to the pristine. Though electrospinning technique is effective in the synthesis of fibrous nanoparticles, Senthamizhan et al. hinted shrinkage and distortions of fabricated

materials, hydrophobic nature, inadequate mechanical properties, poor porosity as some few constraints. The use of polymers and polymeric surfactants in electrospinning results in the reduction of active sites for photocatalytic activity even these surfactants helps to control morphology. ^[76] This synthesis technique produces nanofibers with controlled morphologies on nanoscale with high surface area and surface characteristics. Instrumentation has varying degrees of cost and synthesis process has varying degrees of difficulty in operation. The limitation of this method is finding suitable precursors and the process can be slow.

3.4. Other Synthesis Methods

A combination of methods such as hydrothermal, deposition by DC-pulsed sputtering, atomic layer deposition (ALD), and photo-electrodeposition, [77] electrospray technique hydrothermal, [78] sol-gel, hydrothermal, and microwave-assisted crystallization, [41] were used to fabricate complex composites and heterogenous iron titanate materials. High energy ball milling top-down process was successfully used to synthesize MgO or Mg doped FeTiO₃ using MgO or metallic Mg as doping precursors. [2] Ajmal et al. synthesized Fe₂TiO₅/CN-DP_{10.0} heterojunction nanoparticles for photocatalytic activity. A simple synthesis route was used to prepare carbon nitrile (CN). CN-DP_{10.0} was prepared by the same route by reacting CN with urea resulting in formation of diamino purine (DP) in the structure. Pristine Fe₂TiO₅ is finally incorporated into the structure by mixing in desired solvent. The synthesized composite performed better as compared to carbon nitride which demonstrates low photocatalytic performance in solar energy conversion for photocatalytic water splitting. [22] Triplelayered ITO/BiVO₄/Fe₂TiO₅ heterojunction was synthesized using cathodic deposition, spin coating and annealing techniques. Fluorine-doped tin oxide substrate was coated with ITO as underlayer and Fe₂TiO₅ overlayer and decoration with pristine BiVO₄, [79] forming a photoanode made of a BiVO₄ layer sandwiched between an ITO underlayer as an electron transport layer and a Fe₂TiO₅ overlayer as a hole transport layer yielding a very high photocurrent density of 6.19 mA/ cm² (1.23 V vs. RHE) due to improve charge carrier transfer. [79] Photo-assisted electrodeposition was employed in depositing Co-Pi on the surface of the a-Fe₂O₃/Fe₂TiO₅. [60] Microwave-assisted crystallization contributed in the synthesis of Fe₂TiO₅/TiO₂^[41] for enhancement of photocatalytic properties.

A combination of anodization process, and spin-coating for formation of quaternary FeNiO $_x$ /H $_2$ -treated/TiO $_2$ /Fe $_2$ TiO $_5$ exhibited enhanced photocatalytic properties. Cr, Fe-doped TiO $_2$ and Fe-doped TiO $_2$ were synthesized via radio-frequency magnetron sputtering and colloidal crystal template route respectively to increase the yield of hydrogen gas as compared

to the pristine. Thin films formation of Fe_2TiO_5/α - Fe_2O_3 is aided by synthetic processes such as pulsed laser deposition, [81] whiles a combination of hydrothermal, deposition by DC-pulsed sputtering, atomic layer deposition, photo-electrodeposition techniques favored the engineering of $ITO/Fe_2O_3/Fe_2TiO_5/FeNiOOH$ heterostructure films. [77] Each of these deposition techniques introduces uniqueness in the atomic arrangements leading to efficient charge transfer and other electronic properties for effective catalysis.

Electrospray technique which offers advantages such as precipitation on nanoscale, emulsion diffusion advantage, double-emulsification, and possible provision of layer by layer NPs, simple and low-cost technique, conservation of solvents due to small volumes required, and it being a one-step technique^[82] assisted in fabrication of F-Fe₂TiO₅. ^[83] Kuang et al. synthesized FeOOH/Al-Fe₂TiO₅ by employing electrospray, and hydrothermal technique, [78] and cathodic deposition together with spin coating helped to fabricate ITO/BiVO₄/ Fe₂TiO₅/Fe-silicate photocatalyst.^[79] Zn-Doped Fe₂TiO₅ was formed using aerosol-assisted chemical vapor deposition method. [1] Extremely high photocurrent density of 2.2 mAcm⁻² obtained for ITO/Fe₂O₃/Fe₂TiO₅/FeNiOOH as compared to 0.205 mA cm⁻² (pristine Fe₂O₃) at 1.23 V vs. RHE shows that a well-engineered heterostructure material has enhanced electronic properties suitable for photocatalytic properties. These methods will be beneficial if other photocatalytic properties such as redox potential, low charge recombination rate and stability are also favored. Other applications, results and effectiveness of these engineered materials have been discussed in the application section. Advantages of other synthesis techniques (laser deposition, chemical vapor deposition, sputtering, ball milling, microwave assisted, electrospray techniques) are producing pure and highly crystalline materials, high reproducibility, excellent control of morphology and particle sizes. However, these techniques employs sophisticated instrumentation, high energy requirements, sometimes strict reaction and operational conditions are required, release of dust and toxic materials, mostly produces materials with low porosity. [84,85]

Among these general nanoparticles synthesis techniques, the sol-gel method can be more suitable for synthesis of iron titanate photocatalysts. The sol-gel method can offer unique flexibility to modify precursors and reaction conditions to enhance light absorption and charge transport properties of iron titanate photocatalysts for efficient activity. Moreover, the mode of application of the photocatalyst, composition of solvent medium for water splitting, type and intensity of light, reactor, and experimental design, among other factors can influence the choice of synthesis technique. Composites and heterostructures of iron titanate materials can effectively be fabricated using a combination of techniques or well controlled synthesis methods.

Review THE CHEMICAL RECORD

4. Morphology Controlled of Iron Titanate Nanoparticles

As observed in the synthesis techniques, different synthesis techniques produce some degree of uniqueness in the material fabricated, ranging from high surface area to porosity. Morphology and control of nanomaterial physical characteristics affects the photocatalytic properties and performance. [86] Morphologies of iron titanate materials synthesized in this review include zero dimensional (0D) structures; [2,72,64] onenanowires, [14,38,77] dimensional (1D) which include nanorods, [71,87] nanotubes, [19,23,88] and nanofibers; [37,73] twodimensional (2D)include which films^[22,47,59–61,66,69,89,78,79,81,83] and nanocone; ^[75] and three-dimensional (3D)[38,41,70,68] which mostly formed as layered or agglomerated solid particles. Large surface area is a key property of photocatalytic materials for effective photocatalysis due to the exhibition of large active sites. 1D and 2D fabricated materials possess few atomic-thick layer(s) which offers effective interaction of light and water molecules with photocatalyst material for improvement of catalytic yield. [90] The 3D materials possess low surface area; however, the nanoporous 3D materials have multiple steps and kinks which could be beneficial for catalytic reaction. Capping agents (surfactants) have over the years been used in the fabrication of porous iron titanate photocatalysts as it contributes immensely to tuning morphologies and particle size. [91-93]

5. Application of Iron Titanate Nanoparticles for Water Splitting

The efficiency of the iron titanate photocatalyst is measured in terms of photocurrent generated at the photoelectrode or the amount of hydrogen generated from the reaction set up. Charge or photocurrent density, apparent quantum yield and solar-to-hydrogen conversion efficiency are used to evaluate the efficiency of the catalyst. The amount of hydrogen produced is reported by most findings in moles of gas per hour per gram of photocatalyst.

Though most articles reported the effectiveness of fabricated iron titanate photocatalysts in terms of photocurrent density, Table 1 below highlights the amount of hydrogen generated in water splitting when iron titanate-based catalysts are used.

Three inverse opal structured layers of Fe_2TiO_5 electrode having sacrificial gallium oxide underlayer and a ternary (Ni₂CoFe)OOH co-catalyst resulted in a photocurrent of 2.08 mAcm⁻² at 1.23 V_{RHE} under 1 sun (100 mWcm⁻²) irradiation. [47] Ga_2O_3 underlayer increased the current density of the electrode from 0.49 mAcm⁻² to 1.06 mAcm⁻². The current density increased as the Fe_2TiO_5 layers increased.

Ilmenite FeTiO₃ yielded H₂ production was 296.9 and 265.2 µmol g⁻¹ h⁻¹ of H₂ gas with MgO and metallic Mg doping respectively as compared with 255.3 µmol g⁻¹ h⁻¹ for the undoped FeTiO₃ using UV radiation. Even though there was increase in the bandgap from 2.55 eV to 2.59 eV after doping, there was more negative conduction band potential which favors H₂ production. [2] Fe₂TiO₅ surface treatment with SnO_x coating yielded a photocurrent of 0.36 mA/cm² at 1.23 V vs RHE and 0.64 mA/cm² at 1.8 V as compared to 0.1 mA/cm² at 1.23 V vs RHE and 0.28 mA/cm² at 1.75 V for the pristine Fe₂TiO₅. [66] An amount of 137, 116 and 89 mmol/g catalyst hydrogen was obtained after 6 min residence time for 20, 40 and 60 wt.% Fe respectively in the presence of cobalt. However, only 29 mmol H₂/g catalyst was observed for the pristine TiO₂ nanotubes.^[19] This shows the effect of doping and the importance of weight in doping.

Formation of layered double hydroxide (LDH) containing Fe and Co on the surface of the titanate nanowires (TNWs) as reported by Sayed et al. increased the photocurrent to 3 mA/ cm² at 1 V vs Ag/AgCl from 0.33 mA/cm². A pure LDH sample produced a photocurrent of 1.38 mA/cm² at 1 V vs Ag/AgCl. Anodic current also increased by 9.4, 23.45 and 34.32 folds for the 0.25:1, 0.5:1 and 1:1 photoanodes respectively. [14] The synthesized nanotube photoanode produced a photocurrent density of 0.93 $\mathrm{mA\,cm^{-2}}$ at 1.23 $\mathrm{V}_{\mathrm{RHE}}$ under 1 sun (100 mW cm⁻²) irradiation, which corresponds to 2.6 times that of usual Fe₂TiO₅ photoanode. [23] The photocatalytic H₂ evolution of the co-doped Fe-Ni/TiO₂ synthesized by Sun et al. increased from 249.58 361.64 µmol·h⁻¹·gcat ⁻¹ (with a measured time of 6 h) as compared to pristine TiO₂, Fe/TiO₂, Ni/TiO₂ and catalysts.^[72] Chen et al. reported that the introduction of a Co/Pi catalyst resulted in a photocurrent density of ~3.05 mA/cm² which is higher than the as-prepared photoanode which gave a photocurrent density of ~2.0 mA/cm² (1.23 V vs. RHE).^[60]

Iron intercalated into titanium dioxide to model iron titanate nanotube electrode yielded a photocurrent with ca. 50 mA/cm² at 0.65 (vs. SCE) about 1.5 times faster than the pristine titanium dioxide electrode with a photocurrent of ca. 33 mA/cm²).^[88] Al-Enizi et al. observed 0.38 mol in 14 min of H₂ evolution with the use of TiO₂@CNFs electrode whiles FeTiO₃/TiO₂@CNFs electrode produced 2.97 mol under visible light irradiation. In dark conditions, FeTiO₃/ TiO₂@CNFs electrode generated 1.87 mol of H₂ gas in 14 min of activity as compared to 2.97 mol/14 min obtained visible light illumination. This confirms the enhancement of light absorbing property of the FeTiO₃/ TiO2@CNFs material after composite formation, and the significant amount of H2 gas generated in the dark makes it a promising material for dark photocatalysis. [73] H₂ yielded by the fabricated graphene-assisted titanate nanowires loaded with copper (GP/Cu/TNW) were higher than the other three

Table 1. Hydrogen generation results from the use of iron titanate NPs in mol per hour per gram of catalyst.

No.	Photocatalyst	Synthesis method	Morphology/ band gap	Amount of H ₂ released	Type of light used	Ref.
1.	Mg-FeTiO ₃ , MgO-FeTiO ₃	High Energy Ball Milling (HEBM)	Spherical nanoparticles (2.55–2.59 eV)	240.5 (unmilled), 255.3 (milled) 296.9 (MgO) 265.2 (metallic Mg)] μmol g ⁻¹ h ⁻¹	UV irradiation	2
2.	Fe/Co-Ti ₃ O ₇	Hydrothermal	Nanotube (2.65 eV)	1517 mmolH ₂ g ⁻¹ h ⁻¹	visible light	19
3.	Fe-Ni/TiO ₂ (5.0 % Fe-4.0 % Ni/TiO2)	Solvothermal	Spherical (2.41 eV)	361.64 μmol g ⁻¹ h ⁻¹ after 6 h. Ethanol scavenger	visible light	72
4.	FeTiO ₃ /TiO ₂ @CNFs	Electrospinning method	Nanofibers	0.38 mol (TiO ₂ @CNFs) 2.97 mol (FeTiO ₃ /TiO ₂ @CNFs) in 14 min,	visible light	73
5.	(Ag, Cu, Fe, or Ni) - TiO ₂	Hydrothermal	Nanowires	5 mmol g ⁻¹ after 5 h (Fe- TiO ₂)	visible light	94
6.	(Si,Fe)-TiO ₂	Sol-gel-solvothermal method	Nanocrystalline powders	1800 umol g ⁻¹ (Si,Fe)-TiO ₂) 300 mol g ⁻¹ (Pure TiO ₂) after 6 h	visible light	62
7.	Fe— Ag/TiO ₂ (4.5 % Fe—4.5 % Ag/TiO ₂)	Solvothermal	Polycrystalline structured NPS	515.45 umolg ⁻¹ h ⁻¹ Ethanol scavenger	visible light	70
8.	Fe ₂ TiO ₅ /CN-DP _{10.0}	Simple synthesis route	Irregular nanosheets (2.55 eV)	165.7 μmol/h	visible light	22
9.	Fe/TiO ₂	Hydrothermal	Uniform spherical nanoparticles	12.5 mmol- H_2 /h (methanol) 1.8 mmol- H_2 /h (pure water)	visible light	64
10.	Cr, Fe-doped TiO ₂	Radio-frequency magnetron sputtering and a sol-gel method	Thin films	15.5 µmol h ⁻¹ No hole scavenger	UV-Vis	61
11.	Fe-doped TiO ₂	Colloidal crystal template method	3D well-ordered macroporous structure	25.5 μ mol g ⁻¹ h ⁻¹ Na ₂ S and Na ₂ SO ₃ scavenger	visible light	80
12.	$H:TiO_2$ decorated with Ag, Co, Cr, Cu, Fe, Ni, Pd, Pt and Y	Hydrothermal, Wet impregnation, Thermal hydrogen reduction	Nanofibers	Pd—H:TiO ₂ NFs at a rate of ~17,000 μmol/g·h under UV-A irradiation and at ~25,600 μmol/g·h under UV-B irradiation. Fe showed improved rate than Co, Cr and Cu.	UV-A and UV-B illumination	95
13.	Fe-Ni/Ag/TiO2	Solvothermal	Irregular spherical nanoparticles	793.86 μ mol g ⁻¹ h ⁻¹ for 6 hours. Pure TiO2 for 9.57 μ mol g ⁻¹ h ⁻¹	visible light	96
14.	NaFeTiO4	Simple mixing technique	Rod-like nanoparticles	445 μmol h ⁻¹	visible light	97
15.	FeTiO ₃ / Fe ₂ TiO ₅	Sol-gel method	Mesoporous particles (Honeycomb)	$40.66 \text{ mmol g}^{-1} \text{ h}^{-1}$ $(\text{FeTiO}_3/\text{Fe}_2\text{TiO}_5)$, $23.78 \text{ mmol g}^{-1} \text{ h}^{-1}$ (TiO ₂ -P25)	UV irradiation	98

reference catalysts, the titanate (TiO_2) , titanate nanowires (TNW), and graphene-assisted titanate nanowires without copper (GP/TNW), which is attributed to both increased visible light absorption and efficient charge separation. [94] Impressively, 22 mmol g⁻¹ of H₂ gas was produced after 5 h of illumination. [94]

From the photocatalytic H_2 evolution reaction, Si/Fecodoped sample yielded about 1800 umol/g of H_2 gas after 6 h. The (Si, Fe) codoping contributed to reducing the bandgap for electrons excitation from the VB to CB compared with the pure TiO_2 under the solar light illumination. [62] The use of 4.5% Fe and 4.5% Ag in the synthesis of co-doped

TiO $_2$ as a catalyst yielded an average H_2 production rate by 515.45 umol h $^{-1}$ g $^{-1}$ cat (a measured time of 6 h, visible light irradiation, $\gamma > 400$ nm). About 3000 umol/g of H_2 gas was produced after 6 h. $^{[70]}$ Gao et al. reported that after surface modification of the BiVO $_4$ with Fe $_2$ TiO $_5$, the BiVO $_4$ /Fe $_2$ TiO $_5$ photoanode resulted in a 300 mV cathodic shift in onset potential. BiVO $_4$ /Fe $_2$ TiO $_5$ electrode generated a photocurrent density of 3.2 mA/cm 2 at 1.23 V vs RHE which is 3 times enhancement in photocurrent as compared to Fe $_2$ TiO $_5$. $^{[68]}$ Fe $_2$ TiO $_5$ /CN-DP $_{10}$ exhibited an apparent quantum yield of 61.7% at a wavelength of 420 nm, together with a photocatalytic hydrogen evolution rate of (165.7 µmol/h) along with

15280951, 2024, 5, Dowloaded from https://olinieibrary.wielyc.com/doi/10.002/hc 202400016 b Bishnu Bastaktai - North Carolina A&T State University , Wile Online Library on [0508/2025]. See the Terms and Conditions (https://olinieibrary.wiely.com/doi/10.002/hc 202400016 b Bishnu Bastaktai - North Carolina A&T State University , Wile Online Library on [0508/2025]. See the Terms and Conditions (https://olinieibrary.wiely.com/doi/10.002/hc 202400016 b Bishnu Bastaktai - North Carolina A&T State University , Wile Online Library on [0508/2025]. See the Terms and Conditions (https://olinieibrary.wiely.com/doi/10.002/hc 202400016 b Bishnu Bastaktai - North Carolina A&T State University , Wile Online Library on [0508/2025]. See the Terms and Conditions (https://olinieibrary.wiely.com/doi/10.002/hc 202400016 b Bishnu Bastaktai - North Carolina A&T State University , Wile Online Library on [0508/2025]. See the Terms and Conditions (https://olinieibrary.wiely.com/doi/10.002/hc 202400016 b Bishnu Bastaktai - North Carolina A&T State University , Wile Online Library on [0508/2025]. See the Terms and Conditions (https://olinieibrary.wiely.com/doi/10.002/hc 202400016 b Bishnu Bastaktai - North Carolina A&T State University , Wile Online Library on [0508/2025]. See the Terms and Conditions (https://olineabray.wiely.com/doi/10.002/hc 202400016 b Bishnu Bastaktai - North Carolina A&T State University , Wile Online Library on [0508/2025]. See the Terms and Conditions (https://olineabray.wiely.com/doi/10.002/hc 202400016 b Bishnu Bastaktai - North Carolina A&T State University , Wile Online Library on [0508/2025]. See the Terms and Conditions (https://olineabray.wiely.com/doi/10.002/hc 202400016 b Bishnu Bastaktai - North Carolina A&T State University , Wile Online Library on [0508/2025]. See the Terms and Conditions (https://olineabray.wiely.com/doi/10.002/hc 202400016 b Bishnu Bastaktai - North Carolina A&T State University , Wile Online Library on [0508/2025]. See the Terms and Conditions (https://olineabray.wiely.com/doi/10.002

oxygen (6.2 µmol/h) in the visible spectrum at 420 nm. As compared to the pristine CN (9.9 µmol/h and 0.5 µmol/h), Fe₂TiO₅/CN-DP₁₀ showed 15.7 and 11.4 times higher. A photocurrent density of 4.60 mA/cm² was observed for the ITO/BiVO₄/Fe₂TiO₅ photoanode at 1.23 V_{RHE} which is higher than the pristine BiVO₄ photoanode result of 1.70 mA/cm. A cm. A

FTO/α- Fe₂O₃:Ti/α-Fe₂O₃ photoanode electrode yielded a photocurrent density of 1.69 mA/cm² at 1.9 V vs. RHE under air mass (AM) of 1.5G irradiation. This result is 4.3 times higher than undoped α-Fe₂O₃/α-Fe₂O₃ nanorod (0.39 mA/cm²) and far higher than titanium doped double layered α-Fe₂O₃ nanorod films. ^[69] The inverse opals fabricated using 250 nm PS spheres exhibited higher photocurrent density as compared to the Fe₂O₃, TiO₂ and disordered Fe₂TiO₅ film controls. This was attributed to the enhanced light absorption and increased charge separation. [59] Comparably, Fe₂TiO₅ thin film showed larger anodic photocurrent than the Fe₂O₃ film when coated either on a planar substrate or on nanocone substrate. Fe₂TiO₅ loaded on either planar ITO substrate or nanocone ITO substrate exhibited better (1.4 times larger) than that from Fe₂O₃. [75] Ti and P comodified hematite exhibited a photocurrent of 2.37 mA/cm² at 1.23 V vs. RHE which is higher than the pristine hematite photocurrent of 0.85 mA/cm². Coupling with cobalt phosphate catalyst, denoted as Co-Pi, resulted in the hematite achieving a stable, high photocurrent of 2.90 mA/cm² at 1.23 V vs. RHE.[89]

6. Enhancing the Catalytic Performance

Bassi et al. confirmed that there is lack of complete catalyst fulfilling all the necessary requirements for the highest yield of H₂ generation as well as stability even though there has been great improvements. [66] The perfect semiconductor materials must possess qualities listed but not limited to;

- be abundance, low-cost and non-toxic,
- have a good water oxidation/reduction potential gap,
- exhibit a wide absorption property of light for excitation of electrons.
- have a good charge transport properties with low electronhole recombination rate after electron excitation,
- illustrate great stability thermally, mechanically and in the reaction medium.

Due to the semiconductor properties and good chemical stability in aqueous solutions, metal oxides have been identified as the most promising catalysts. Reported efficiencies of these NPs are however still low for commercialization purposes. [1] Even though iron titanate NPs such as pseudobrookite (Fe_2TiO_5), which is a hybrid of hematite (Fe_2O_3) and TiO_3 having Fe-O-Ti bonds, more studies are being

conducted to fully understand its properties. With a low bandgap of about 1.9-2.1 eV and a promising n-type semiconductor was expected from Fe₂TiO₅ as a photocatalyst but Regue et al. reported challenges in synthesis and the lack of complete knowledge of its properties as some hinderances to discovering its full photocatalytic potential.^[1] Computational and DFT studies are ongoing to aid in the understanding of the properties of these NPs. [99] The interface between two semiconductor solids has been observed to usually generate a thermal boundary resistance in Ohmic contact, a challenge that hinders effective charge transfer. Nanoengineering of heterogeneous interfaces with tunable energy band position has been identified to be beneficial for suppressing charge recombination and promoting the transport of holes and electrons. As expected, Zhang et al. reported a photocurrent density of the optimized hierarchical TiO₂/Fe₂TiO₅/Fe₂O₃ (abbreviated as TFF) inverse opal value of 0.54 mA cm⁻² at 1.23 V vs. RHE, far higher than the pristine TiO₂/Fe₂O₃ (abbreviated as TF) inverse opal (0.02 mA cm⁻² at 1.23 V vs. RHE). [49] It has been projeted that there are more than 700,000 possible combinations for ternary and quaternary metal oxide NPs, which is paving way to finding that ideal NPs for use as effective photocatalyst for high efficiency as well generating hydrogen gas at a lower cost as substitute for fossil fuels. Future research opportunities therefore opens to identify that ideal photocatalytic material. [47] Some excellent NPs have been investigated and reported in literature with great advancement for PEC performance and charge separation efficiency is as high as 61.0% for the TFF inverse opals. [49]

6.1. Doping and co-Doping

Owing to the need to improve the photocatalytic properties of pristine ${\rm TiO_2}$ and other compositions, doping is employed in the fabrication of photocatalysts. Doping improves the electronic and optical properties [37,100] of photocatalysts as confirmed by Lin et al. in the synthesis of (Si/Fe-codoped ${\rm TiO_2}$ which improved hydrogen generation due to synergistic effects between the Si, Fe and ${\rm TiO_2}$ which effectively induce the red shift of optical absorption edge thereby enhancing visible-light absorption. [62] As shown in Figure 8(b), co-doping decrease the band gap and shifted the conduction band to a more negative potential facilitating reduction of ${\rm H^+}$ for hydrogen gas formation. [62]

Co-doping TiO₂ by Mahmoud et al. resulted in shift of absorption edge 365 nm to 600 nm enhancing visible light photocatalysis. ^[19] One of the highest focuses of photocatalysis is the aim to shift the conduction band level of photocatalysts to enhance the photocatalytic performance of the photocatalysts towards effective hydrogen evolution reactions. Khlyustova et al. reported and impressive enhancement in photocatalytic activity to 70% after addition of aluminum and

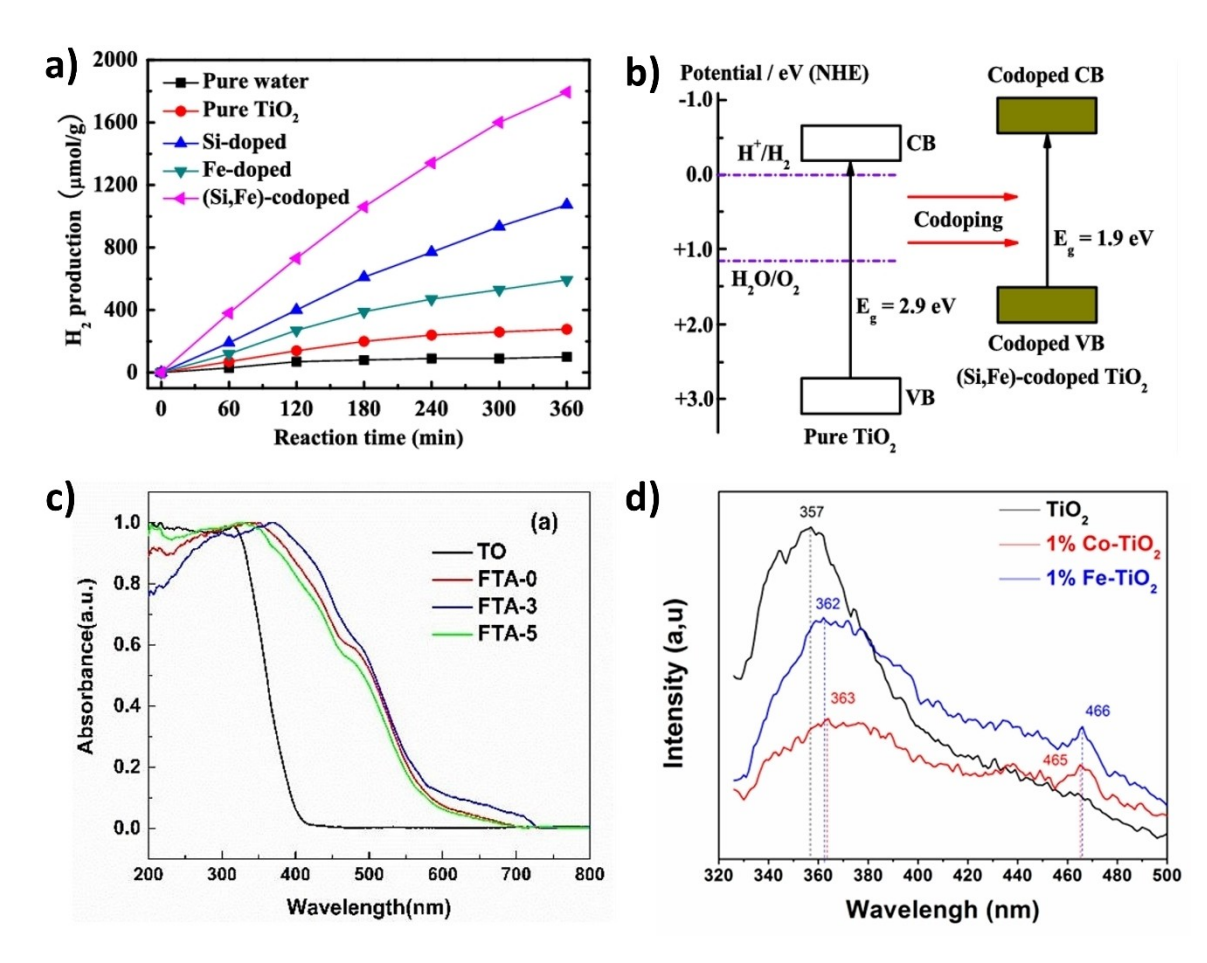


Figure 8. a) Yield of hydrogen increased through doping, $^{[62]}$ b) Shifting of electronic bands and lowering of band gap through doping, $^{[62]}$ c) Enhanced light absorption due to modification of TiO_{2} , $^{[37]}$ and d) Photoluminescence spectrum. Low emission at about 360 nm indicating reduction in recombination of photogenerated electrons and holes through Fe or Co doping, $^{[100]}$

copper as dopants and the results became enhanced by a rise in the activity to 96% after doping with Mo. [101] This confirms the importance of elemental doping of photocatalysts semiconductors towards effective photocatalytic activity. Nonmetal doping has also been identified as an efficient means to reduce band gap. Doping of N and S into lattices has been reported to contribute to reducing the band gap of TiO_2 for visible light absorption. [28] Petit et al. stated the importance of factoring and modifying synthesis to include the arrangement of ions in a nanostructure enhanced photocatalytic performance. [41] Co-doping of Fe_2TiO_5/Fe_2O_3 with fluorine and ruthenium yields an improved photocurrent of 1.47 mA/cm² at 1.0 V vs. RHE, 3 times more than that of the pristine Fe_2TiO_5/Fe_2O_3 . [102]

Extensive researches have been done to enhance the photocatalytic activity of TiO₂ by doping with transition metal atoms that have unpaired electrons in the 3d orbital (M=V, Cr, Mn, Fe, Co, Ni, Cu, and Zn) or 4d unpaired electrons (M=Y, Zr, Nb, Mo, and Ag). [19,103] With reference to various

transition metal oxides, ternary metal oxides have been identified to exhibit multiple oxidation states making them undergo multiple redox reactions. [104] The addition of dopants into the crystal lattice either results in p-type or n-type material. Dopants are introduced in small amounts which can result in effective improvement in the photocatalytic properties of the semiconductors. [105]

Though metals have been widely targeted as dopants and literature has reported more on metal doping and co-doping, non-metal doping of transition metal oxides for visible-light photocatalysis is also widely practiced in recent times due to their ability to reduce large band gap of photocatalysts materials to effectively absorb visible light. [106] Carbon, sulphur, nitrogen, and fluorine have been frequently used in doping among the non-metals. Carbon has been reported to minimize the bandgap of TiO₂ by producing a hybrid orbital over the valence level of TiO₂ and resulting in improved visible light absorption. [107] Sulphur creates localized states in the energy band gap structure of TiO₂ when doped, which helps

to reduce bandgap. These localized states improves electronic transition upon visible light illumination with enhances optical properties. [108,109] Nitrogen improves the transfer of photogenerated electrons when used as a dopant. [110] Fluorine is reported to introduce energy states below the O 2p valence band when doped into ${\rm TiO_2}$ leading to the formation of ${\rm Ti^{3+}}$ ions. [111] In general, the incorporation of elements as dopants causes distortion of the ${\rm TiO_2}$ or the iron titanate crystal lattice resulting in variation of their surface characteristics, and consequently reducing the band gap. [112] The reduction in band gap further leads to enhancement of optical, electronic, and photocatalytic properties.

6.2. Heterogeneous Material Fabrication

The need to acquire the appropriate conduction band of semiconductors toward hydrogen generation has been one of the key reasons for modification of photocatalyst semiconductors. As displayed in the Figure 9, the level of the conduction band must be more negative than the redox potential of H⁺/H₂ (0 V vs. normal hydrogen electrode (NHE)), and the top level of the valence band must be more positive than the redox potential of O₂/H₂O (1.23 V vs. NHE). [44] Composite formation from two or more catalysts helps to enhance this property. Cañas et al. experimented with the generation of hydrogen using FeTiO₃ NPs under UV irradiation. Based on results from the unmilled sample (240.5 μmol g⁻¹ h⁻¹), it was evident that milling increased the surface area with improved yield (255.3 μmol g⁻¹ h⁻¹) which

further increased to 296.0 μ mol g⁻¹h⁻¹ (milled with 1.0 wt% MgO), and 265.2 μ mol g⁻¹h⁻¹ (milled with 1.0 wt% metallic Mg). This enhancement of the photocatalytic yield was due to the increase in the surface area and formation of composite which subsequently modifies the band structure to improve the optical and electrochemical properties. ^[2] Regue et al. engineered thin layers of Fe₂TiO₅ on top of TiO₂ and α -Fe₂O₃ to enhance photocatalytic properties. The synthesis of Fe₂TiO₅ and a CoO_x catalyst composite on top of TiO₂ nanotubes increased the incident-photon-to-current efficiency from 5% to 40% using light of wavelength of 400 nm and +1.23 V RHE, displaying an enhancement in charge carrier transport within the synthesized NPs. ^[1]

Apart from binary catalyst or metal oxides which have two elements, most semiconductors for catalytic purposes are recently being fabricated to have three (ternary) or four (quaternary) different elements in the semiconductor system. Ouaternary semiconductor systems are now gaining more attention. Liu et al. reported that ternary system contributes in enhancement of photocatalytic activity during photocatalytic water splitting. [113] Formation of composites forms heterojunction which enhanced charge separation as a result of suitable band alignment.[114] Wang et al. reported that Fe₂TiO₅/Fe₂O₃/Pt composite synthesized has an excellent photo response due to heterojunction formation resulting in efficient water splitting. The effective charge separation, charge transport as well as adequate light harvesting are key areas of focus.[115] When the synergistic effect of the composite, and hence the heterostructure formed, supersedes the individual

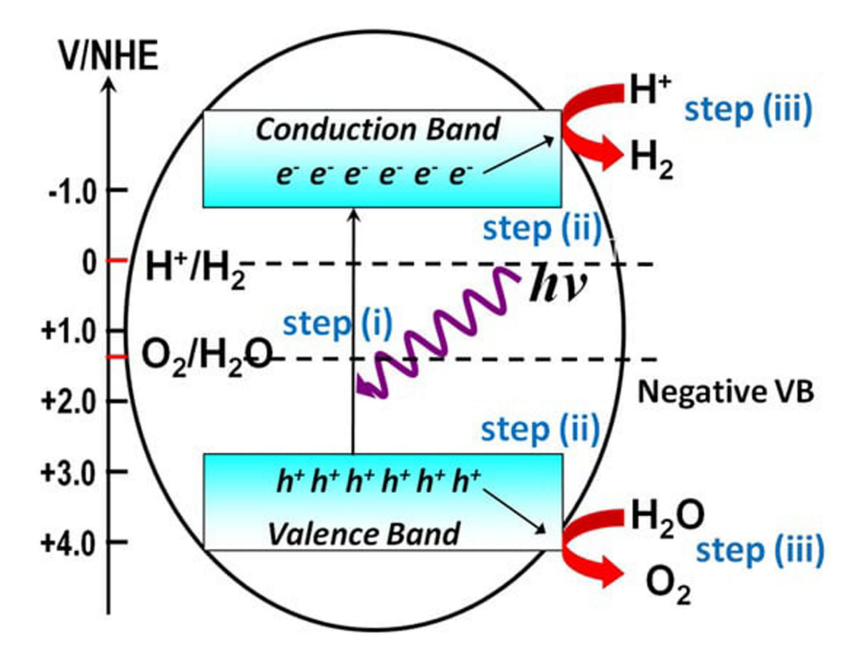


Figure 9. Schematic representation of conduction and valence band alignment. [44]

nanoparticles improved photocatalytic properties are achieved. It has been reported that many approaches have been put in place to improve the solar-to-hydrogen conversion efficiency and subsequently improve hydrogen evolution reaction rate and yield. Elemental doping, heterojunction formation, defects, and interfacial engineering mechanisms are a few approaches found to be helpful in achieving high efficiency. [49] Numerous attempts have been made and future progress is again focusing on depositing different photocatalytic species on fabricated NPs to build interfacial heterojunctions including type I heterojunctions, Schottky junctions, and Ohmic junctions as reported by Zhang et al.. [49] More crystalline samples are being fabricated since photocatalytic activity is observed to be enhanced by the crystallinity of the photocatalyst. Ways to decrease the density of states and recombination activities of charge are also being exploited. [45]

6.3. Tuning Band gap

The band gap of the semiconductor which refers to the separation between the conduction band minimum and the valence band maximum was determined for photocatalysts to investigate their conductivity and to help understand other optical and electrochemical behaviors. Fe₂TiO₅, as an n-type semiconductor, has narrow band gap of about 2.1 eV which explains its ability to absorb visible light. [47] Yang et al. used UV-Vis diffuse reflection spectroscopic technique to study the light absorption properties of synthesized samples. Though TiO₂ poorly absorbs light with a wavelength of more than 400 nm, the combination of Fe₂TiO₅ with TiO₂ lowered the band gap and improved the absorbance of the composite. The absorption visible light further improved when Ag was added to the composite (Ag/TiO₂/Fe₂TiO₅). This confirms that introducing dopants and composites enhances the band gap of semiconductor NPs. Peng et al. synthesized Fe₂TiO₅-TiO₂ nanocages (NCs) with a band gap of 2.1 eV with an enhanced light absorption in a broad band of solar spectrum. As anode materials, these NCs effectively when used in photoelectrochemical (PEC) water splitting. [71] Some nanoparticles have been investigated to have more negative conduction band values which are suitable for hydrogen evolution reaction. MgTiO3 is an example with a good conduction band at a more negative potentials. [116] However, as compared to FeTiO₃ with a band gap between 2.59-2.9 eV, a wide band gap of MgTiO₃ between 3.4–3.7 eV^[2] makes it unsuitable for use as photocatalyst in the visible light region since lots of energy is needed for its activation. Though incorporating Mg and MgO into the crystal lattice of FeTiO3 increased the band gap, the overall synergistic effect resulted in the shifting of the conduction band of Mg/FeTiO₃ and MgO/FeTiO₃ composites to a more negative potential for enhanced H₂ generation.

6.4. Experiment Design (Condition and Scavenger Molecules)

Sun et al. observed an improved performance in hydrogen gas generated from 249.58 to $361.64\,\mu mol\,g^{-1}\,h^{-1}$ after adding ethanol as the sacrificial agent to the reaction medium. A low yield of 1.8 mmol-H₂/h hydrogen generated using pure water as compared to 12.5 mmol-H₂/h in aqueous methanol indicating the contribution of sacrificial agents (scavengers) in hydrogen production. The use of water as proton source without the help of sacrificial agent will be a challenge and proposed the optimization of reaction conditions such as environment temperature as well as use of sacrificial agents in controlled amount. The design of suitable photoreactors also have been identified to play a role in photocatalytic mechanism. In photocatalytic mechanism.

Sacrificial agents have been proven to improve the H₂ efficiency. [118,119] Though sacrificial agents serve as electron donors or hole scavengers and minimizes electron-hole recombination, reactors design can focus on mechanisms to eliminate products from hole scavengers by continuously feeding with controlled amounts of scavenger molecules or creating a scavenger-water flow system to replace solution within the reactor. Interference from products of sacrificial agents will be eliminated when solution is gradually replaced. This can be beneficial to accelerate the rate of hydrogen generation since effective rate of hole scavenging is required to enhance photoactivity. Reverse hole transfer investigation by Zao et al. with different hole scavengers proved that methanol with short chain hydrocarbon is a better hole scavenger. [120] As an advantage, methanol was used as sacrificial agents, yields some amount of hydrogen after getting oxidized, and forms formaldehyde, formic acid which are also sacrificial agents for water splitting.

6.5. Surface Area

As a measure of the total area occupied by all surfaces of a given solid, surface area plays a key role in catalysis. Being one of the pioneers of active site catalysis investigations, Hugh Stott Taylor was said to be the first to report that only active sites of a fabricated nanoparticle are involved in a catalytic reaction and not the entire surface as reported by Vogt and Weckhuysen. Nanoparticles exhibit enhanced catalytic properties as a result of high surface area compared to the bulk material. From the review, researchers targeted engineering materials possessing 0D, 1D or 2D morphologies due to their large surface areas. Nanotube, and nanofibers morphologies saw appreciable yield of H₂ gas in the range of millimoles per hour per gram of catalyst due to high surface area as compared to the polycrystalline structure reporting 515.45 umolg⁻¹h⁻¹ of H₂ gas. Tolerate and surface area as compared to the polycrystalline structure reporting 515.45 umolg⁻¹h⁻¹ of H₂ gas.

possess porosity to allow the interaction of solvent molecules with more active sites within the structure. Small pore sizes and large surface area of nanoparticles contribute to the enhancement of their optical, physical, and chemical properties required for effectiveness. [122,123]

The photocatalytic performance of iron titanate NPs in hydrogen evolution reaction has been observed to improve simply by milling the samples (from 240.5 255.3 µmol g⁻¹ h⁻¹), due to the increase in surface area of the NPs^[2]. Bassi's proposed the need for fabrication of thicker films to aid in absorption of more light. However, thin films are known to be better absorption of light than thick films as confirm by Sreekanth et al. [124] due to large surface area. The advantages offered by thick films lie in porosity and crystal arrangement of the semiconductor. Well-formed, porous, and thick films will allow light penetration and enough light harvesting for enhanced photocatalytic activity. Fe₂TiO₅-TiO₂ nanocages fabricated by Zhang et al. with hollow structures possess beneficial light absorption property and improved surface area for enhanced photocatalytic activity. [38]

6.6. Limitations and Future Perspective

Grey, turquoise, blue, black or brown types of H₂ generate CO₂ as by-products; pink H₂ generates nuclear waste and green H₂ from electrolysis tend to be energy intensive making green H₂ from photocatalysis cost effective and environmentally friendly. Most photocatalytic investigations from iron titanate lack report on shortfalls associated with its use for H₂ generation. However, lots of previous reports are centered on improving limitations associated with TiO₂; high electronhole recombination, inefficient exploitation of visible light, wide band gap and stability issues. In this regard, some limitations and future perspective shall include but not limited to:

- Creation of sequential configurations for n-type and p-type materials are necessary during composite formation as this will enhance electron-hole transfer. The nature of material arrangements during synthesis can contribute significantly to the kinetics of the charge transfer and suppression of electrons and holes recombination. Fabricating n-type to ptype to n-type to p-type sequencing can yield effective charge transfer.
- 2. Combining elements with multiple oxidations states [copper (+1, +2), cobalt (+2, +3), titanium (+3, +4), iron (+2, +3), manganese (+2, +3, +4, +6, +7), vanadium (+2, +3, +4, +5), chromium (+2, +3, +6), molybdenum (multiple but stable at +4, +6) and tungsten (multiple but stable at +4, +5)] will aid in the release of efficient charges for redox activities which is key in photocatalysis. Doping and forming composites with these

- metals increases the electron density and subsequently improves the charge transfer within the semiconductor.
- 3. In addition to computational and density functional theory (DFT) studies, detailed investigation can be carried out focusing on variation of experimental conditions, elemental composition, crystallinity, and morphology and studying the corresponding effects on the optical, magnetic, and electronic properties of the photocatalyst semiconductors.
- 4. Investigating hydrogen evolution activity using varying compositions and concentrations of sacrificial agents and varying the degree of purity of water used in hydrogen generation as pollutant water is being reported to perform better than deionized water.
- 5. Heterojunction formation improves charge transfer and migration whiles reducing electron-holes recombination. A stronger synergistic effect must exist within the components in the heterostructure and must supersede the individual nanoparticles performance to achieve enhanced activity.

7. Conclusion

In conclusion, the pivotal role played by materials in facilitating water splitting towards hydrogen generation has generated greater attention in the field of photocatalysis. As hydrogen gas is currently in production and usage in pilot bases, the need for scale up and low-cost production is calling for more research into suitable catalysts for large scale and lowcost production. The shortfalls of TiO2 effective photocatalysis have resulted in numerous modifications over the years. This review has critically evaluated the effect of incorporating iron into the crystals lattice of TiO2 to form iron titanate photocatalyst and highlighted advances made in their synthesis, morphology, and application towards hydrogen production, and elaborated on future prospects. When the field is advanced, iron titanate will be one of the best and more economical photocatalyst for water splitting due to its abundance, low-cost, non-toxicity, recoverability, environmental friendliness, and easy handling.

This review has made detailed emphasis ways to improve the efficiency in the use of iron titanate as a photocatalyst. Synthesis modifications during material fabrication, factors to consider in experimental design, DFT simulations have been highlighted as ways to improve the efficiency of iron titanate photocatalysts. These techniques is aimed at providing useful insight to aid in future research, modification and application of iron titanate in photocatalysis for hydrogen evolution. Again, as highlighted in this review based on the previous works, intense investigation into fabrication of advanced materials with desired compositions and architectures will be more applicable for enhancement of hydrogen evolution activities via water splitting in the presence of light. As previous works has basically proven that modification of TiO₂

with iron to produce iron titanate photocatalysts improved photocatalytic yield as compared to the pristine ${\rm TiO_2}$, and further modification of the iron titanate showed better performance, there is the assurance that further studies will yield potential materials in future. These modifications, when well investigated into, can help to achieve or closely reach the goal of settling on that excellent material, that is stable, cost-effective, and exhibiting most photocatalytic properties for integration into the current cutting-edge findings for sustainable, renewable and clean H_2 gas for the future generation.

Acknowledgements

This work is supported by the National Science Foundation (NSF) Research Initiation Award (NSF-RIA 2000310). MS was supported by the NSF Partnerships for Research and Education in Materials (NSF-PREM 2122067). DK and BB were supported partially in the summer by the Center for Electrochemical Dynamics and Reactions on Surfaces via grant DE-SC0023415.

Conflict of Interest

The authors declare that they have no known competing financial interests or personal relationships that could have appeared to influence the work reported in this paper.

References

- M. Regue, I. Y. Ahmet, P. S. Bassi, A. L. Johnson, S. Fiechter, R. Van De Krol, F. F. Abdi, S. Eslava, ACS Appl. Energ. Mater. 2020, 3, 12066.
- [2] D. M. Cańas, M. Sandra, C. Díaz, M. Manrique, R. Gómez, J. A. P. Avella, *Top. Catal.* **2021**, *64*, 2.
- [3] O. Vozniuk, N. Tanchoux, J. M. Millet, S. Albonetti, F. Di Renzo, F. Cavani, Spinel Mixed Oxides for Chemical-Loop Reforming: From Solid State to Potential Application, 1st ed., Elsevier B. V., 2019, 178, 281.
- [4] S. Kumar, D. D. Rodene, R. B. Gupta, *Renewable Sustainable Energy Rev.* **2018**, *89*, 228.
- [5] J. Yang, A. Sudik, C. Wolverton, Chem. Soc. Rev. 2010, 37, 656.
- [6] B. C. Tashie-lewis, S. Godfrey, Chem. Eng. J. Adv. 2021, 8, 100172.
- [7] U. S. Dep. Energy Hydrogen, Energy.gov, Office of Energy Efficiency & Renewable Energy, Hydrogen and Fuel Cell Technologies, https://www.energy.gov/eere/fuelcells/hydrogenstorage.
- [8] H. Ge, F. Xu, B. Cheng, J. Yu, W. Ho, *ChemCatChem* **2019**, *11*, 6301.
- [9] L. Vermillion, Control Mag. 2023. https://www.controlglobal. com/home/article/11288233/batteries-or-fuel-cells-for-energy-storage.

- [10] Senza 2023, *Power from water* **2023**. doi:https://senzahydrogen.com/hydrogen-vs-lithium.html.
- [11] S. Palanisamy, S. Srinivasan, A. P. Shyma, N. Rajendhran, K. Subramani, V. Murugan, R. Venkatachalam, SN Appl. Sci. 2019, 1, 1.
- [12] Z. Z. Vasiljevic, M. P. Dojcinovic, J. D. Vujancevic, I. Jankovic-Castvan, M. Ognjanovic, N. B. Tadic, S. Stojadinovic, G. O. Brankovic, M. V. Nikolic, R. Soc. Open Sci. 2020, 7, 200708.
- [13] J. Huang, Y. Cao, Z. Liu, Z. Deng, F. Tang, W. Wang, Chem. Eng. J. 2012, 1807, 5.
- [14] R. A. Sayed, S. E. Abd, E. Ha, N. Gamal, Y. Gadelhak, W. M. A. El Rouby, *J. Alloys Compd.* 2017, 728, 1171.
- [15] T. Helmenstine, CRC Handb. Chem. Physics, 89th Ed. 2021.
- [16] J. Robert R. Seal II, Klaus J. Schulz, John H. DeYoung, U. S. Geol. Surv. Prof. Pap. 2017, 1802, 797.
- [17] D. Nattanmai, R. Vettumperumal, R. Arunmetha, J. Mater. Sci. Mater. Electron. 2020, 31, 16951.
- [18] A. Fujishima, K. Honda, Nature 1972, 238, 37.
- [19] M. S. Mahmoud, E. Ahmed, A. A. Farghali, A. H. Zaki, N. A. M. Barakat, *Mater. Chem. Phys.* 2018, 217, 125.
- [20] N. R. Mucha, J. Som, S. Shaji, S. Fialkova, P. R. Apte, B. Balasubramanian, J. E. Shield, M. Anderson, D. Kumar, J. Mater. Sci. 2020, 55, 5123.
- [21] N. R. Mucha, J. Som, J. Choi, S. Shaji, R. K. Gupta, H. M. Meyer, C. L. Cramer, A. M. Elliott, D. Kumar, ACS Appl. Energ. Mater. 2020, 3, 8366.
- [22] Z. Ajmal, A. Hayat, M. Qasim, A. Kumar, A. E. Jery, W. Abbas, M. B. Hussain, A. Qadeer, S. Iqbal, S. Bashir, Z. Ahmed, J. Qian, A. Murtaza, H. Zeng, Sustain. Mater. Techno. 2023, 36, e00594.
- [23] H. Zhang, J. H. Kim, J. H. Kim, J. S. Lee, Adv. Funct. Mater. 2017, 27, 1702428.
- [24] H. A. Centurion, M. A. Melo, L. G. Rabelo, G. A. S. Alves, W. S. Rosa, I. Rodríguez-Gutiérrez, F. L. Souza, R. V. Gonçalves, J. Alloys Compd. 2023, 933, 167710.
- [25] T. Imrich, H. Krýsová, M. Neumann-Spallart, J. Krýsa, Catal. Today 2023, 413–415, 113982.
- [26] M. Rafique, S. Hajra, M. Irshad, M. Usman, M. Imran, M. A. Assiri, W. M. Ashraf, ACS Omega 2023, 8, 25640.
- [27] Amika, R. Sharma, A. Sharma, A. Chandrani, J. Singh, D. Kumar, J. Phys. Conf. Ser. 2022, 2267, 012016.
- [28] H. H. Do, D. L. T. Nguyen, X. C. Nguyen, T. Le, T. P. Nguyen, Q. T. Trinh, S. H. Ahn, D. N. Vo, S. Y. Kim, Q. V. Le, Arab. J. Chem. 2020, 13, 3653.
- [29] M. A. Aziz Aljar, M. Zulqarnain, A. Shah, M. S. Akhter, F. J. Iftikhar, AIP Adv. 2020, 10, 070701.
- [30] dimensions.ai, https://app.dimensions.ai/discover/publication.
- [31] W. Peng, Y. Chen, J. He, S. Ou, R. Ho, Sci. Rep. 2018, 145, 1.
- [32] E. Chikoidze, T. Tchelidze, E. Popova, P. Maso, N. Ponjavidze, N. Keller, Y. Dumont, Appl. Phys. Lett. 2013, 102, 122112.
- [33] M. K. Nowotny, P. Bogdanoff, T. Dittrich, S. Fiechter, A. Fujishima, H. Tributsch, *Mater. Lett.* 2010, 64, 928.
- [34] A. Bally, Mater. Sci. Phys. Eng. 1999, 2094, 140.

15280691, 2024, 5, Downloaded from https://onlinelibrary.wiley.com/doi/10.1002/tcr.202400016 by Bishnu Bastakoti - North Carolina A&T State University, Wiley Online Library on [05/08/2025]. See the Terms conferms-and-conditions) on Wiley Online Library for rules of use; OA articles are governed by the applicable Creative Commons Licensu

- [35] M. Ntoukakis, A. Pantinakis, A. Vafidis, T. Markopoulos, Appl. Sci. 2019, 9, 3310.
- [36] M. K. Nowotny, L. R. Sheppard, T. Bak, J. Nowotny, J. Phys. Chem. C 2008, 112, 5275.
- [37] F. Yang, X. J. Yu, T. Zhang, J. F. Niu, J. Li, J. K. Nie, J. P. Li, B. H. Yao, *IOP Conf. Ser.: Earth Environ. Sci.* 2019, 344, 012096.
- [38] P. Zhang, X. F. Lu, D. Luan, X. Wen, D. Lou, Angew. Chem. 2020, 132, 8205.
- [39] J. Fu, Q. Xu, J. Low, C. Jiang, J. Yu, Appl. Catal. B 2019, 243, 556.
- [40] F. L. Souza, An. Acad. Bras. Cienc. 2018, 90, 745.
- [41] S. Petit, S. T. A. G. Melissen, L. Duclaux, M. T. Sougrati, T. Le Bahers, P. Sautet, D. Dambournet, O. Borkiewicz, C. Laberty-robert, O. Durupthy, U. De Lyon, E. Normale, D. Lyon, U. Claude, B. Lyon, L. De Chimie, J. Phys. Chem. C 2016, 120, 24521.
- [42] Q. Duc, J. Liu, C. Chung, Y. Ling, Catal. Commun. 2012, 19, 85.
- [43] B. Gao, Y. J. Kim, A. K. Chakraborty, W. I. Lee, Appl. Catal. B 2008, 83, 202.
- [44] X. Zhang, H. Liu, J. Xu, T. Ji, W. Zong, Catalysts 2023, 13, 729.
- [45] M. B. Tahir, M. Rafique, M. S. Rafique, M. Sagir, M. Maraj, A. Jabeen, S. Zahid, A. Batool, *Micro and Nano Tech.* 2020, 139–158.
- [46] P. Kumar, S. Mulmi, Y. Huang, S. Wei, D. Kong, M. Wang, J. Phys. Conf. Ser. 2022, 2267, 012016.
- [47] H. Zhang, S. O. Park, S. H. Joo, J. H. Kim, S. K. Kwak, J. S. Lee, *Nano Energy* 2019, 62, 20.
- [48] C. Ros, T. Andreu, J. R. Morante, J. Mater. Chem. A 2020, 8, 10625.
- [49] M. Zhang, P. Liu, H. Tan, H. Zhang, F. Huang, K. Zhang, S. Li, Sci. China Mater. 2021, 65, 124.
- [50] M. Ni, M. K. H. L. Á, D. Y. C. Leung, K. Sumathy, Renewable Sustainable Energy Rev. 2007, 11, 401.
- [51] A. T. Raghavender, N. Hoa Hong, K. Joon Lee, M. H. Jung, Z. Skoko, M. Vasilevskiy, M. F. Cerqueira, A. P. Samantilleke, J. Magn. Magn. Mater. 2013, 331, 129.
- [52] S. F. Shaikh, M. Ubaidullah, R. S. Mane, *Types, Synthesis methods and applications of ferrites, Elsevier Inc., Micro and Nano Tech.*, **2020**, 52.
- [53] M. K. Bhattarai, M. D. Ashie, S. Dugu, K. Subedi, B. P. Bastakoti, G. Morell, R. S. Katiyar, *Molecules* 2023, 28, 1914.
- [54] J. Bentley, S. Desai, B. P. Bastakoti, Chem. A Eur. J. 2021, 27, 9241.
- [55] S. Munkaila, R. Dahal, M. Kokayi, T. Jackson, B. P. Bastakoti, Chem. Rec. 2022, 22.
- [56] B. P. Bastakoti, N. Bhattarai, M. D. Ashie, F. Tettey, S. I. Yusa, K. Nakashima, *Polymer* **2023**, *15*, 1739.
- [57] E. Yilmaz, M. Soylak, Functionalized nanomaterials for sample preparation methods, Elsevier Inc., Modern Trends in Analysis, 2019, 375.
- [58] L. Liu, Z. Zhao, Z. Hu, X. Lu, S. Zhang, L. Huang, Y. Zheng, H. Li, Front. Chem. 2020, 8, 371.
- [59] X. An, H. Lan, R. Liu, H. Liu, J. Qu, New J. Chem. 2017, 41, 7966.

- [60] S. Chen, Q. Zeng, J. Bai, J. Li, L. Li, L. Xia, B. Zhou, Appl. Catal. B 2017, 218, 690.
- [61] R. Dholam, N. Patel, M. Adami, A. Miotello, Int. J. Hydrogen Energy 2009, 34, 5337.
- [62] Y. Lin, Z. Jiang, C. Zhu, X. Hu, H. Zhu, X. Zhang, J. Fan, S. Hsien, Int. J. Hydrogen Energy 2013, 38, 5209.
- [63] E. Courtin, G. Baldinozzi, et al., J. Mater. Chem. A 2014, 2, 6567.
- [64] M. A. Khan, S. Ihl, O. Yang, Int. J. Hydrogen Energy 2008, 33, 5345.
- [65] A. D. Li, W. C. Liu, Phys. Prop. Appl. Polym. Nanocomposites 2010, 108.
- [66] P. S. Bassi, S. Y. Chiam, J. Barber, L. H. Wong, ACS Appl. Mater. Interfaces 2014, 6, 22490.
- [67] W. K. Jo, Y. J. Jin, J. Alloys Compd. 2018, 765, 106.
- [68] Y. Gao, Y. Li, G. Yang, S. Li, N. Xiao, B. Xu, S. Liu, P. Qiu, S. Hao, L. Ge, ACS Appl. Mater. Interfaces 2018, 10, 39713.
- [69] T. Kong, J. Huang, X. Jia, W. Wang, Y. Zhou, Appl. Surf. Sci. 2019, 486, 312.
- [70] T. Sun, E. Liu, J. Fan, X. Hu, F. Wu, W. Hou, Y. Yang, Chem. Eng. J. 2013, 228, 896.
- [71] Z. Peng, et al, Angew. Chem. Int. Ed. 2020, 59, 8128.
- [72] T. Sun, J. Fan, E. Liu, L. Liu, Y. Wang, H. Dai, Y. Yang, W. Hou, *Powder Technol.* 2012, 228, 210.
- [73] A. M. Al-enizi, A. Yousef, M. Ubaidullah, A. Karim, M. M. El-Halwany, J. King Saud Univ. Sci. 2023, 35, 102538.
- [74] G. K. Sharma, N. R. James, Synth. Met. 2023, 296, 117376.
- [75] K. Chen, T. Duy, T. Duc, H. Dang, A. Tamanai, S. Ishii, X. Li, H. Misawa, T. Nagao, *Nano Energy* **2020**, *76*, 104965.
- [76] L. Jia, X. H. Qin, J. Therm. Anal. Calorim. 2013, 112, 595.
- [77] P. Tang, H. B. Xie, C. Ros, L. J. Han, M. Biset-peiri, Y. M. He, W. Kramer, A. P. Rodriguez, E. Saucedo, J. R. Galan-Mascaros, T. Andreu, J. R. Morante, J. Arbiol, *Energy Environ. Sci.* 2017, 10, 2124–2136.
- [78] S. Kuang, M. Wang, Z. Geng, X. Wu, Y. Sun, D. Chen, J. Liu, S. Feng, K. Huang, ACS Sustainable Chem. Eng. 2019, 7, 14347.
- [79] Q. Sun, L. Qi, Chem. Eng. J. 2021, 426, 131290.
- [80] X. Yan, C. Xue, B. Yang, G. Yang, Appl. Surf. Sci. 2017, 394, 248.
- [81] M. Osada, K. Nishio, K. Lee, M. Colletta, B. H. Goodge, W. J. Kim, L. F. Kourkoutis, H. Y. Hwang, Y. Hikita, ACS Appl. Energ. Mater. 2021, 4, 2098.
- [82] J. A. Tapia-herna, P. I. Torres-cha, M. Plascencia-jatomea, C. G. Barreras-urbina, N. A. Rangel-va, J. Agric. Food Chem. 2015, 63, 4699.
- [83] M. Wang, X Wu, Nanoscale 2018, 14, 6678-6683.
- [84] N. Kaur, M. Singh, A. Moumen, G. Duina, E. Comini, *Materials* 2020, 13, 2974.
- [85] P. G. Jamkhande, N. W. Ghule, A. H. Bamer, M. G. Kalaskar, J. Drug Delivery Sci. Technol. 2019, 53, 101174.
- [86] B. P. Bastakoti, Y. Li, T. Kimura, Y. Yamauchi, Small 2015, 11, 1992.
- [87] S. Farhoosh, B. Eftekharinia, M. Tayebi, B. Lee, N. Naseri, Appl. Surf. Sci. 2021, 550, 149374.
- [88] J. Suk, D. Hyun, S. Hee, J. Wook, H. Gyu, J. Sung, Int. J. Hydrogen Energy 2012, 37, 11081.

15280691, 2024, 5, Downloaded from https://onlinelibrary.wiley.com/doi/10.1002/tcr.202400016 by Bishnu Bastakoti

A&T State University, Wiley Online Library on [05/08/2025]. See the Terms

of use; OA articles are governed by the applicable Creative Commons License

- [89] X. Lv, K. Nie, H. Lan, X. Li, Y. Li, X. Sun, J. Zhong, T. Lee, Nano Energy 2017, 32, 526.
- [90] H. Wang, X. Liu, P. Niu, S. Wang, J. Shi, L. Li, Matter 2020, 2, 1377.
- [91] Y. Li, B. P. Bastakoti, V. Malgras, C. Li, J. Tang, J. H. Kim, Y. Yamauchi, *Angew. Chem.* 2015, 127, 11225.
- [92] Y. Li, B. P. Bastakoti, M. Imura, S. M. Hwang, Z. Sun, J. H. Kim, S. X. Dou, Y. Yamauchi, *Chem. A Eur. J.* 2014, 20, 6027.
- [93] B. P. Bastakoti, S. Ishihara, S. Y. Leo, K. Ariga, K. C. W. Wu, Y. Yamauchi, *Langmuir* 2014, 30, 651.
- [94] W. Jo, Y. Jin, J. Alloys Compd. 2018, 765, 106.
- [95] M. C. Wu, W. K. Huang, T. H. Lin, Y. J. Lu, Appl. Surf. Sci. 2019, 469, 34.
- [96] T. Sun, E. Liu, X. Liang, X. Hu, J. Fan, Appl. Surf. Sci. 2015, 347, 696.
- [97] D. S. Shinde, P. D. Bhange, S. S. Arbuj, J. Y. Kim, J. H. Bae, K. W. Nam, S. N. Tayade, D. S. Bhange, *Int. J. Hydrogen Energy* **2020**, *45*, 8605.
- [98] M. D. Ashie, B. P. Bastakoti, Small 2024, 2310927, 1.
- [99] P. Makkar, N. N. Ghosh, RSC Adv. 2021, 11, 27897.
- [100] A. E. Mragui, Y. Logvina, L. P. da Silva, O. Zegaoui, J. C. G. E. da Silva, *Materials*. 2019, 12, 3874.
- [101] A. A. A. Khlyustova, N. Sirotkin, T. Kusova, A. Kraev, V. Titov, Mater Adv 2020, 1, 1193.
- [102] J. Z. Jiujun Deng, X. Lv, K. Nie, X. Lv, X. Sun, ACS Catal. 2017, 7, 4062.
- [103] Y. Wang, R. Zhang, J. Li, L. Li, S. Lin, Nanoscale Res. Lett. 2014, 9, 1.
- [104] G. S. Di Chen, Q. Wang, Wanga, J. Mater. Chem. A 2015, 3, 10158–10173.
- [105] C. Libretexts, Chem. Libr. 2023. Semiconductors band gaps, colors, conductivity and doping. Chem. Libr. 2023, doi: info@libretexts.org.
- [106] R. Marschall, L. Wang, Catal. Today 2014, 225, 111.
- [107] T. Fotiou, T. M. Triantis, T. Kaloudis, K. E. O'Shea, D. D. Dionysiou, A. Hiskia, Water Res. 2016, 90, 52.

- [108] M. Bettinelli, V. Dallacasa, D. Falcomer, P. Fornasiero, V. Gombac, T. Montini, L. Romanò, A. Speghini, *J. Hazard. Mater.* 2007, 146, 529.
- [109] C. Yu, D. Cai, K. Yang, J. C. Yu, Y. Zhou, C. Fan, J. Phys. Chem. Solids 2010, 71, 1337.
- [110] R. Shi, Z. Li, H. Yu, L. Shang, C. Zhou, G. I. N. Waterhouse, L. Wu, T. Zhang, *ChemSusChem* **2017**, *10*, 4650.
- [111] C. Foo, Y. Li, K. Lebedev, T. Chen, S. Day, C. Tang, S. C. E. Tsang, *Nat. Commun.* 2021, 12, 1.
- [112] A. Khlyustova, N. Sirotkin, T. Kusova, A. Kraev, V. Titov, A. Agafonov, Mater Adv 2020, 1, 1193.
- [113] E. Liu, C. Xu, C. Jin, J. Fan, X. Hu, J. Taiwan Inst. Chem. Eng. 2019, 97, 316.
- [114] P. Saurabh, R. P. Antony, P. P. Boix, Y. Fang, J. Barber, L. Helena, *Nano Energy* 2016, 22, 310.
- [115] L. Wang, N. T. Nguyen, X. Huang, P. Schmuki, Y. Bi, Adv. Funct. Mater. 2017, 27, 1703527.
- [116] X. Yong, M. A. A. Schoonen, Am. Mineral. 2000, 85, 543.
- [117] S. Tasleem, M. Tahir, Renewable Sustainable Energy Rev. 2020, 132, 110073.
- [118] C. Ai, J. Shi, S. Hu, J. Li, B. Luo, Int. J. Hydrogen Energy 2022, 47, 15149.
- [119] T. Zhang, S. Lu, Chem Catal. 2022, 2, 1502.
- [120] J. Zhao, R. Shi, Z. Li, C. Zhou, T. Zhang, Nano Sel. 2020, 1, 12.
- [121] C. Vogt, B. M. Weckhuysen, Nat. Chem. Rev. 2022, 6, 89.
- [122] S. M. M. Alonzo, J. Bentley, S. Desai, B. P. Bastakoti, Sci. Rep. 2023, 13, 1.
- [123] S. K. Ray, B. Pant, M. Park, B. P. Bastakoti, J. Anal. Appl. Pyrolysis 2023, 175, 106207.
- [124] K. V. Sreekanth, M. ElKabbash, V. Caligiuri, R. Singh, A. D. Luca, G. Strangi, New Direction in Thin Film Nanophotonics; Springer Singapore, 2019.

Manuscript received: January 17, 2024 Revised manuscript received: April 6, 2024 Version of record online: May 22, 2024